10 Muon-Spin Rotation (μSR) and Magnetization Studies of Superconducting Materials

H. Keller, C. Aegerter, J. Hofer, M. Hunt (till Jan. 97), V.A. Ivanshin (visiting scientist), S. Romer (since Feb. 97), A. Shengelaya (since March 96), M. Willemin, G.M. Zhao, and K.A. Müller (Honorarprofessor)

10.1 Introduction

In the work carried out over the past year we have continued our detailed study of the magnetic properties of high-temperature superconductors and related magnetic systems. In order to achieve this goal we have used a combination of muon spin rotation (μSR), electron paramagnetic resonance (EPR), together with bulk SQUID and torque magnetometry measurements, and thermal expansion measurements.

The μSR technique probes the local internal field distribution in the mixed state of a superconductor. Over the past years this technique has been applied, among other things, to understanding the microscopic arrangements of flux vortices and associated transitions (flux-lattice melting) in highly anisotropic superconductors, where significant progress has been achieved. In the last year we have continued our μSR studies of $Bi_2Sr_2CaCu_2O_8$ (BSCCO), in which we intend to investigate the exotic vortex behavior at a microscopic level, and extended these studies to highly anisotropic organic superconductors and BSCCO containing columnar defects induced by irradiation with heavy ions (see Sec. 10.2).

The nature of the symmetry of the superconducting pair wave function is a fundamental question of current interest. In order to test the pairing symmetry we have carried out precise measurements of the ab-anisotropy of $Tl_2Ba_2Cu_3O_{6+x}$ films by means of a specially designed torque sensor based on a silicon lever (see Sec. 10.3.1). In addition, we have improved the design and the performance of our recently constructed nano-torque magnetometer (see Annual Report 95/96). For this purpose we have designed a new type of piezoresitive cantilever, which can simultaneously operate in the flexion and torsion mode and allows calibration measurements with an integrated calibration coil (see Sec. 10.3.2).

EPR is a powerful method to study crystal electric fields and static and dynamic correlations on a microscopic level. Last year this technique has successfully been used the first time to demonstrate an oxygen isotope effect of the ferromagnetic exchange energy in colossal magnetoresistive manganites (see Sec. 10.5.1), providing microscopic evidence for the formation of Jahn-Teller (JT) polarons in doped manganites (see Sec. 10.4). Furthermore, we performed EPR measurements in order to investigate the peculiar magnetic properties of the spin-ladder compound $Sr_{0.72}CuO_2$ at a microscopic level.

We have continued our oxygen-isotope effect studies in the giant magnetoresistance ferromagnetic Jahn-Teller (JT) perovskite $La_{1-x}Ca_xMnO_3$ by means of magnetization and EPR measurements, as well as measurements of the thermal expansion coefficient (see Annual Report 95/96). Our results provide strong evidence for the formation of JT polarons in these materials (see Sec. 10.5.1). Furthermore, we have performed magnetization and thermal expansion measurements on ^{16}O and ^{18}O samples of the cuprate superconductor $La_{2-x}Sr_xCuO_4$ for investigating the isotope effect on the in-plane penetration depth (see Sec. 10.5.2). Our results show that polaronic charge carriers exist and condense into Cooper pairs in the cuprate superconductors, as originally suggested by Bednorz and Müller.

This work was done in collaboration with scientists from ETH Zürich (G. Blatter, K. Conder, and J. Karpinski), IBM Rüschlikon Laboratory (C. Rossel), University of Birmingham (E.M. Forgan and S.H. Lloyd), University of St. Andrews (S.L. Lee and C. Ager), Institut Max von Laue-Paul Langevin, Grenoble (R. Cubitt), University of Oxford (S.J. Blundell), RIKEN-RAL (F.L. Pratt), Tohoku University (T. Sasaki), and Free University of Amsterdam (B. Stäuble-Pümpin).

10.2 μSR measurements of highly anisotropic superconductors

The high-temperature superconducting cuprates show anisotropic superconducting and magnetic behavior. This is largely due to their layered structure, where the currents preferentially flow in the CuO_2 planes. This anisotropy is parameterised by $\gamma = \lambda_c/\lambda_{ab}$, where λ_c and λ_{ab} are the penetration depths for currents flowing perpendicular and parallel to the superconducting planes, respectively. The high-temperature superconductor $Bi_{2.15}Sr_{1.85}CaCu_2O_{8+\delta}$ (BSCCO) shows an extreme anisotropy with γ as high as 200 for optimally doped samples. Therefore in this material a vortex line penetrating the sample is better described by a stack of 'pancake' vortices, each confined to a CuO_2 plane, rather then an extended, three dimensional (3D) object. These 'pancake' vortices interact both within the planes as well as between different adjacent planes. The interactions within the planes originate always from the supercurrents flowing in the CuO_2 planes. Between the planes the interactions can arise from Josephson tunneling currents flowing between the planes or also from screening currents in the adjacent layers. These two cases are referred to as Josephson coupling and electromagnetic coupling, respectively. Usually, Josephson coupling is taken to make up the main part of the inter-layer coupling in high temperature superconductors. However, for extremely anisotropic superconductors, obeying the relation $\gamma s > \lambda_{ab}$, where s is the inter-layer separation, Blatter *et al.* [1] have shown, that the vortex behavior may well be dominated by electromagnetic coupling.

Using μSR we can microscopically probe the vortex distribution in the mixed state of type II superconductors. This is done over the field probability distribution $p(B)$, which is intimately related to the spatial distribution $B(r)$. This has allowed us in the past to observe such interesting phenomena as vortex lattice melting and the dimensionality of the vortex system [2, 3]. This year we have investigated these phenomena further to obtain information on the nature of the inter-layer coupling in the extremely anisotropic BSCCO. Following the analysis of Blatter *et al.* [1], we investigated the field dependence of the melting temperature in detail, as differences are expected for the different types of inter-layer coupling. Especially, there should be a crossover in the shape of the melting line, at the temperature T^{em}, where the criterion for the dominance of electromagnetic coupling breaks down, $\lambda(T^{em}) = \gamma s$. This behavior was indeed observed [4] and allowed us to determine γ to be $\simeq 160$.

The nature of the inter-layer coupling also has interesting consequences on the dimensional crossover field. At this field, there is a strong change in the field distribution p(B) [5] to a more symmetric shape. This has been interpreted as arising from the improved adjustment of pancake vortices to pinning sites, when the inter-layer coupling becomes weaker than the intra-layer coupling. For a system consisting of Josephson coupled pancake vortices a calculation of these properties gives $B_{2D} = \Phi_0/(\gamma s)^2$ [6], where $\Phi_0 = h/2e$ is the flux-quantum. This means that the Josephson coupling is dramatically weakened as the cores of the Josephson vortices associated with the Josephson currents start to overlap. For superconductors such as BSCCO however, where $\gamma s > \lambda_{ab}$ the vortices are still further apart then the typical length scale of their interaction (λ_{ab}), such that they interact very weakly. Hence the electromagnetic inter-layer coupling is still stronger than the intra-plane interactions, delaying the crossover up to a field of $B_\lambda = \Phi_0/\lambda_{ab}^2$, where the vortices are only λ_{ab} apart and therefore interact more strongly. We have investigated the dimensional crossover for a number of samples having different oxygen contents and therefore different penetration depths using μSR. The result is shown in Fig. 10.1, where we have plotted the crossover field as a function of the inverse square of the penetration depth. It can be clearly seen that the crossover field in the samples studied follows the behavior expected from the above discussion. To study the dependence of this dimensional crossover on the anisotropy we have also carried out measurements on BSCCO samples containing columnar defects induced by irradiation with 17.3 GeV U ions. The tracks of these heavy ions act as very strong pinning sites, such that a stack of pancake vortices will be ordered along them effectively increasing the dimensionality of the vortex system. In our μSR and small angle neutron scattering (SANS) measurements we have observed this effect. The field distribution $p(B)$ shows a tail at high fields and there is scattering from extended vortex lines in SANS [9] at fields much higher than the crossover field in the pristine material. Furthermore we have shown that the 2D thermal fluctuations present in the unirradiated samples [3] are strongly reduced in those containing columnar defects [9]. This is due to the fact that the ionic tracks strongly pin the vortices along their length, which is of importance to applications since thermal fluctuations of vortices may lead to resistive behavior. Moreover, we have started an extensive study of the vortex behavior in a superconducting charge transfer salt of the organic

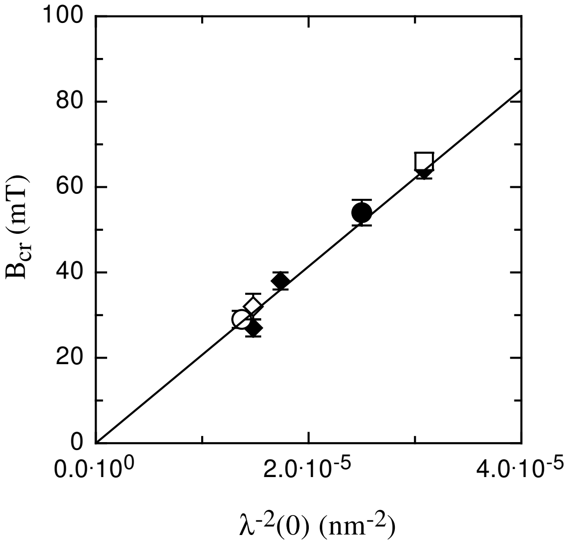

Figure 10.1: The crossover field B_{cr} as a function of $\lambda_{ab}^{-2}(0)$ for different samples of BSCCO. Open symbols correspond to μSR measurements on samples studied in ref. [5]: circle is sample S_1; square S_2; diamond S_3. Filled diamonds are taken from Ref. [7] and are obtained from magnetization measurements using Hall bar arrays. Filled circles are from a Tl-2212 sample taken from Ref. [8], where the crossover field is determined by magnetization measurements. The solid line corresponds to the relation $B_{cr} = \Phi_0/\lambda_{ab}^2$, which describes the data without any adjustable parameter.

molecule bis(ethylenedithio)tetrathiafulvalene (BEDT-TTF or ET). We studied the superconducting material κ-(BEDT-TTF)$_2$Cu(SCN)$_2$ (ET-SCN), with a transition temperature of approximately 10.4 K, that shows extremely anisotropic behavior as BSCCO. We therefore expect to observe a dimensional crossover similar to that in BSCCO. Due to the very long penetration depths (600 nm) in these samples however, there might be some differences with respect to the inter-layer coupling. Our results on ET-SCN, where we observe a dimensional crossover at a field of $\simeq$ 5 mT [10], however are consistent with a mechanism as in BSCCO, where the dominating inter-layer coupling is of electromagnetic nature.

10.3 Magnetization measurements of high-T_c and classical superconductors by torque magnetometry

10.3.1 Pairing symmetry in single-layer tetragonal $Tl_2Ba_2CuO_{6+x}$ from in-plane torque anisotropy

Since the discovery of high-T_c superconductivity several experiments for testing the pairing symmetry in these novel superconductors were performed, but the situation is still controversial. One part of the experiments, such as the phase-sensitive experiments of Tsuei et al. [11] performed with $Tl_2Ba_2CuO_{6+x}$ (Tl2201) and $YBa_2Cu_3O_{7-\delta}$ tricrystals yield evidence for a $d_{x^2-y^2}$ symmetry [12, 13]. On the other hand, a number of experiments, such as the Josephson tunneling experiment along the c-axis of optimally doped $YBa_2Cu_3O_{7-\delta}$ by Sun et al. [14] point to a s-wave symmetry. Recently, Müller [15] has proposed, that in these short-coherence length superconductors two condensates with different symmetry (s- and d-wave), but the same T_c, may be present, in agreement with a large number of experimental results.

In our experiment we studied the in-plane torque anisotropy in a Tl2201 film grown on $SrTiO_3$ (001) by rf magnetron sputtering [16]. Films of two different thicknesses were used. The tetragonal structure of Tl2201, checked at room temperature with x-rays, is certainly an advantage for this kind of experiment, compared to orthorhombic compounds like $YBa_2Cu_3O_{7-x}$. However, we cannot totally exclude a small orthorhombic distortion at low temperature. The films were patterned into disks of 2 mm diameter to avoid geometrical effects. A capacitance torque meter based on a silicon lever allows measurements on thin films grown on substrates with a very good resolution ($\sim 10^{-11}$ Nm) (see insert of Fig. 10.2a, left). The intrinsic background signal induced by the lever is negligibly small. For these measurements the magnetic field has to be applied exactly in the *ab*-plane of the sample to avoid an unwanted contribution from the *c*-axis magnetization (Fig. 10.2a, left). A misalignment less than 0.07° was achieved with a small magnetic field perpendicular to the main external field.

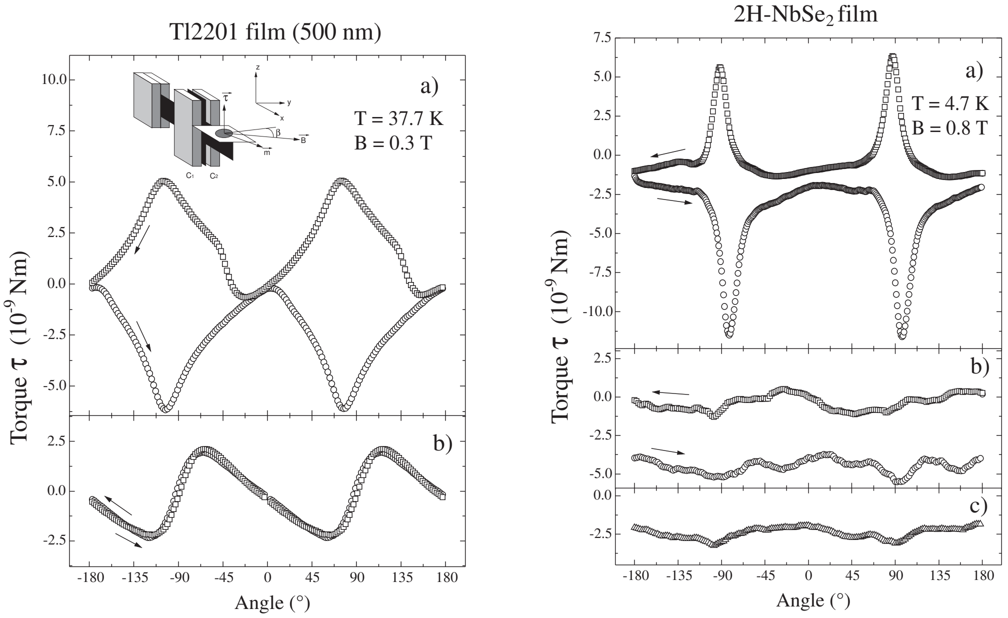

Figure 10.2: Left : a) Out-of-plane torque of a 500 nm-thick Tl2201 film. In this case the c-axis magnetization dominates and the large irreversibility is due to pinning. b) In-plane torque, almost perfectly reversible. Insert: Thin film mounted on the capacitance torque meter. Right : Angular dependent torque of a 2H-$NbSe_2$ film. a) Before proper in-plane alignement of B. b) After alignement corrections. c) Reversible part of the torque.

The comparison of the in-plane torque of the Tl2201 (Fig. 10.2b, left) and the 2H-$NbSe_2$ (Figs. 10.2b and c, right) shows two totally different behaviors. For the conventional superconductor also a pinning contribution in the *ab*-plane was observed, but the reversible torque signal (Fig. 10.2c, right) has almost no structure, which is fully compatible with a pure s-wave symmetry. The almost perfectly reversible in-plane torque signal of the Tl2201 samples shows a structure (independent of film thickness) being very likely due to a mixture of s- and d-wave symmetry. A strong temperature dependence of this structure was observed. However, a convincing theoretical interpretation of our results is not yet found. Similar measurements will be performed on $(NdCe)_2CuO_{4-x}$ films in order to confirm our results.

10.3.2 Design of ultrasensitive piezoresistive cantilevers for torque magnetometry

Silicon microfabricated cantilevers with piezoresistive readout are now successfully used in commercial atomic force microscopes (AFM) [17]. Moreover, it has been shown recently that such levers are very well suited for torque magnetometry [18].

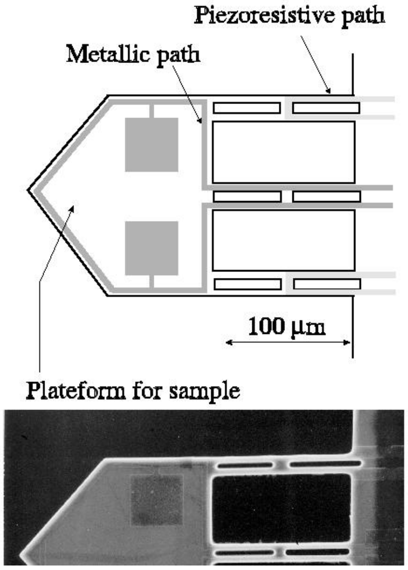

Figure 10.3: Top: Schematic view of the piezoresistive cantilever with the integrated coil for calibration measurements. Bottom: SEM image of the cantilever.

The goal of this new design is to use the lever in flexion as well as in torsion mode in order to detect torque signals with respect to two axes (see Fig. 10.3). A torque being applied to the cantilever will produce a mechanical stress in each leg, which can be detected by a change of the piezoresistances R_1 and R_2. The torque τ_x or τ_y can be extracted by measuring $\Delta(R_1 + R_2)$ or $\Delta(R_1 - R_2)$, respectively. The design and the microfabrication of these devices are the result of a common research project between IBM Research Division Zurich and the Physics Institute of the University of Zurich [19]. The advantages of these cantilevers are the two-axes sensitivity with a particular high resolution in the flexion mode ($\leq 10^{-12}$ Nm for a constant applied torque) and the optimization of the sensitivity ratio between the two modes. For such a geometry the resolution in the torsion mode is always about a factor 5 weaker than in the flexion mode. These microlevers will be very helpful for future investigations of new anisotropic magnetic materials. A systematic study of the *ac*-anisotropy by means of torque magnetometry on mercury compounds $HgBa_2Ca_{n-1}Cu_nO_{2n+2+x}$ (see Annual Report 95/96) was performed during the last year and will be continued using these new levers as well.

10.4 EPR measurements in manganates and cuprates

Electron Paramagnetic Resonance (EPR) is a powerful tool in solid state physics, which allows to study crystal electric fields, electron-phonon interactions, static and dynamic magnetic correlations on a *microscopic* level. EPR is a contactless method, thus samples of any form: powder, pellet, single crystal, thin film can be measured. Also, due to the extreme sensitivity of EPR, only a tiny amount of material is necessary. In 1996 a new EPR spectrometer, kindly donated by Prof. K.A. Müller (IBM Research Laboratory, Rüschlikon), was installed in our laboratory. This is a BRUKER ER-200 spectrometer working at an X-band frequency of about 9.3 GHz and magnetic field sweeping range 0-1.5 T. It is equipped with an Oxford Instruments ESR-900 helium gas-flow cryostat for low-temperature measurements (4-300 K). We have also a special insert for high-temperature measurements, which allows to reach about 800 K.

We performed EPR measurements on colossal magnetoresistive (CMR) manganese based perovskite $La_{1-x}Ca_xMnO_{3+y}$ for ^{16}O and ^{18}O isotope substituted compounds in the paramagnetic regime [20]. A strong symmetric EPR signal with a Lorentzian lineshape was observed. Two typical EPR signals at room temperature are shown in Fig 10.4. Note that the signal of the ^{16}O sample is stronger than that of the ^{18}O sample. This oxygen-isotope effect on the EPR intensity is very unusual and was observed for the first time.

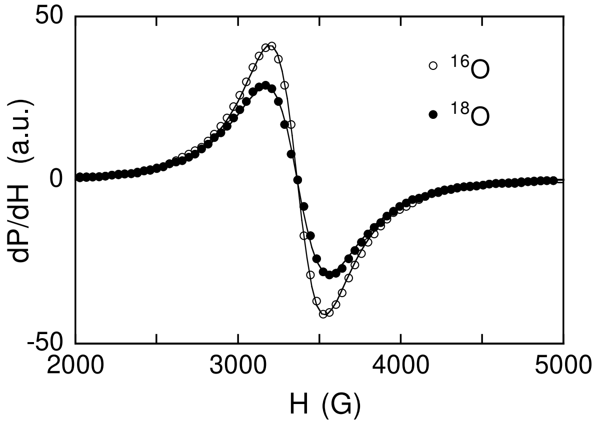

Figure 10.4: EPR signal of ^{16}O and ^{18}O samples of $La_{0.8}Ca_{0.2}MnO_{3+y}$ measured at T=300 K under identical experimental conditions. The fits with a Lorentzian line shape are indicated by solid lines.

The EPR signal of $La_{1-x}Ca_xMnO_{3+y}$ is extremaly strong (no more than 1 mg of samples was used to avoid saturating the spectrometer) and has an unconventional temperature dependence. To understand these unusual EPR features, it is necessary to point out that doped manganese perovskites are mixed-valent systems, containing Mn^{3+} and Mn^{4+} ions with a strong ferromagnetic double exchange interaction between them. We propose that the EPR signal observed in $La_{1-x}Ca_xMnO_{3+y}$ is primarily due to Mn^{4+} ($3d^3$ with S=3/2) ions. In an octahedral anion crystal electric field this ion has a ground state, corresponding to an orbital singlet A_2. Consequently, the spin-lattice relaxation is weak and this makes EPR of Mn^{4+} easy to observe, even at high temperatures [21]. The Mn^{3+} ($3d^4$ with S=2) is unlikely to have an observable EPR signal as it exhibits a large zero-field splitting and strong spin-lattice relaxation (the ground state of Mn^{3+} ion is the orbital doublet) [22]. The characteristic differences observed in the EPR intensity and linewidth for the two isotope samples can be explained by a model in which a bottlenecked spin relaxation takes place from the exchange-coupled constituent Mn^{4+} ions via the Mn^{3+} Jahn-Teller ions to the lattice. For x=0.2 the ferromagnetic exchange energy J exhibits a $^{16}O/^{18}O$ oxygen isotope effect of $\sim$-10%. This difference in J should be compared with the 10% difference of the ferromagnetic Curie temperature T_c observed in these samples (see Sec. 10.5.1) and provides *microscopic* evidence for the formation of JT polarons in doped manganese perovskites.

Recently novel one-dimensional (1D) hole doped cuprates of the form $Sr_{0.72}CuO_2$ were synthesized under high oxygen pressure at ETH Zürich in the laboratory of J. Karpinski [23]. For many decades the spin chains have attracted much attention in condensed matter physics. Due to the enhanced quantum fluctuations in one dimension, they exhibit various interesting quantum magnetic phenomena, which have no analogy in higher dimensions. It is well known that in the high-T_c cuprates superconductivity results when the 2D antiferromagnetic copper-oxygen planes are doped with holes. What happens when one starts to add holes to 1D copper-oxygen chains? In view of the enhanced quantum fluctuations in 1D systems, doping of copper-oxygen chains could well lead to equally surprising discoveries. The $Sr_{0.72}CuO_2$ compound is made of edge sharing CuO_2 chains and the average valency of copper is +2.56. Thus $Sr_{0.72}CuO_2$ provides an unique possibility to study properties of hole doped CuO_2 chains.

Perhaps the most peculiar feature of $Sr_{0.72}CuO_2$ is a sudden jump in the magnetization observed below $\sim$10 K, indicating a ferromagnetic-like magnetic transition [23]. We have performed EPR measurements to study the magnetic properties of $Sr_{0.72}CuO_2$ on a microscopic level. Fig. 10.5 shows the EPR signal observed in $Sr_{0.72}CuO_2$ at different temperatures. The powder averaged spectra with $g_{||}$=2.21(1) and $g_{\perp}$=2.015(5) is characteristic for Cu^{2+} ions in an axial crystal electric field [22].

Considering the crystal structure of $Sr_{0.72}CuO_2$, $g_{||}$ and $g_{\perp}$ correspond to the

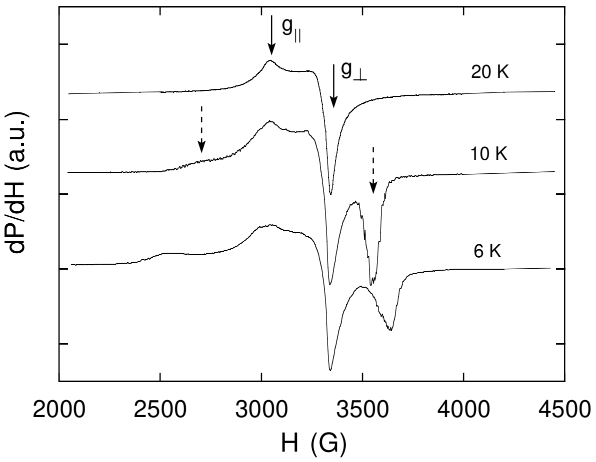

Figure 10.5: EPR spectra of $Sr_{0.72}CuO_2$ at various temperatures. Dashed arrows mark two extra peaks which split from the main EPR line below the magnetic transition temperature.

magnetic field H perpendicular and parallel to the CuO_2 chains, respectively. The g-values and linewidths of the EPR signal are almost temperature independent. However, with decreasing the temperature below ~12 K, two new lines split from the main EPR line (see Fig. 10.5). With decreasing temperature one line splits from the $g_{||}$ peak and shifts to lower fields, while another line splits from the $g_\perp$ peak and shifts to higher fields. It is remarkable that the EPR line splits at the same temperature where the sharp increase of the magnetization was detected, and the splitting is significantly larger that the linewidth. This demonstrates that below T_c a well defined internal field develops in $Sr_{0.72}CuO_2$ due to the long-range magnetic ordering. Further experimental work to clarify the nature of the magnetic transition is still in progress.

10.5 Studies of oxygen isotope effects

10.5.1 Oxygen isotope effects in the manganites

The manganese-based perovskites $La_{1-x}Me_xMnO_3$ (Me = Ca, Sr, and Ba) have recently been the subject of intensive investigations because of their unusual and potentially useful magnetic properties (e.g., the colossal magnetoresistance (CMR) effect [24, 25]). The microscopic mechanism for the CMR has not been clear, and now is being intensively explored. These materials contain a mixture of Mn^{3+} and Mn^{4+} ions at octahedral lattice sites and exhibit a strong Jahn-Teller (JT) effect. Höck *et al.* [26] studied JT ions in a conductor within a linear chain model. They showed that small JT polarons can be formed when the JT stabilization energy is comparable with the bare conduction bandwidth. This important concept led Bednorz and Müller [27] to discover high-temperature superconductivity in cuprates which also have a strong JT effect. The polaronic nature of the conduction carriers can be demonstrated by the isotope effect on the effective bandwidth W_{eff} of polarons, which in turn depends on the isotope mass M [28]. In the ferromagnetic manganites, it is easy to study the isotope effect on W_{eff}. This is due to the fact

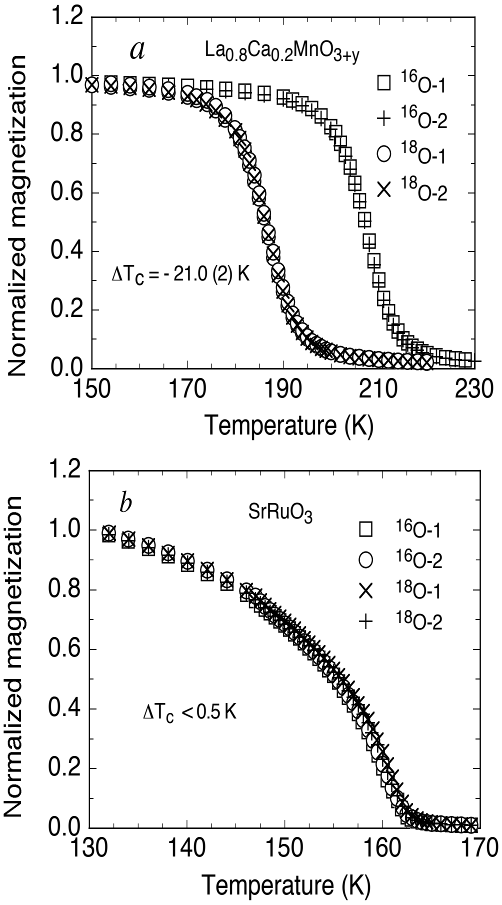

Figure 10.6: Temperature dependence of the normalized magnetization for the ^{16}O and ^{18}O samples of (a) $La_{0.8}Ca_{0.2}MnO_{3+y}$; (b) $SrRuO_3$.

that in the strong-coupling limit, where the Hund's rule coupling J_H is very large compared to W_{eff} ($J_H \gg W_{eff}$), the Curie temperature $T_c \propto W_{eff}$ (Ref. [29, 30]). The isotope dependence of W_{eff} can also be investigated in a ferromagnet $SrRuO_3$, where T_c strongly depends on W_{eff}, as indicated by a large pressure effect [31]. In the ferromagnet $SrRuO_3$, however, the JT effect is very weak, so the isotope dependence of W_{eff} might be very weak. Therefore, studies of the oxygen-isotope effect on the Curie temperature in these ferromagnets can assess the importance of the JT effect in the formation of polarons. We have studied the oxygen-isotope effect on the ferromagnetic transition temperature T_c in the perovskites $La_{1-x}Ca_xMnO_{3+y}$ and $SrRuO_3$ (also see Ref. [32]). As seen from Fig. 10.6, the oxygen-isotope shift of T_c in $La_{0.8}Ca_{0.2}MnO_{3+y}$ is very large (>20 K), far larger than any isotope shift found for magnetic or electronic phase transitions in other oxides. In contrast, no sizable isotope shift was observed in the structurally-related ferromagnet $SrRuO_3$. The results suggest that the charge carriers in manganites are strongly coupled to the JT lattice distortions so that JT polarons are formed.

We have also performed extensive studies of the oxygen-isotope effects in the manganites from magnetization, EPR, thermal-expansion and resistivity measurements. The linear thermal-expansion coefficient $\beta(T)$ exhibits an asymmetric peak

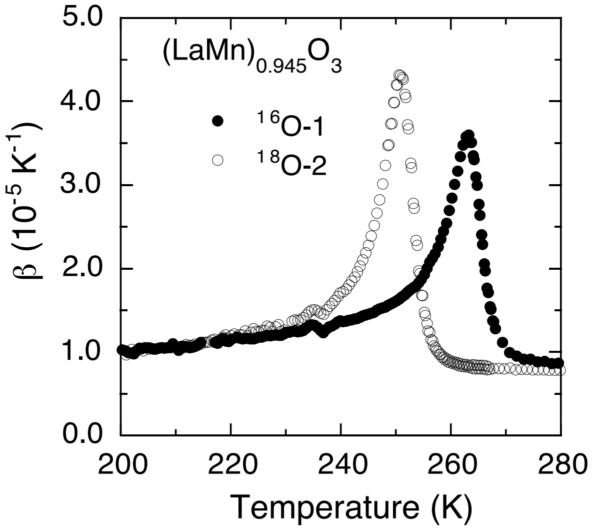

Figure 10.7: The linear thermal-expansion coefficient β(T) for the ^{16}O and ^{18}O samples of $(LaMn)_{0.945}O_3$.

at the Curie temperature T_c of the compounds $(La_{1-x}Ca_x)_{1-y}Mn_{1-y}O_3$ with a Mn^{4+} concentration of ~33%. Upon replacing ^{16}O with ^{18}O, the second-order jump in the thermal-expansion coefficient ($\Delta\beta(T_c)$) is raised by about 20%, as seen from Fig. 10.7. Such a "colossal" oxygen-isotope effect on $\Delta\beta(T_c)$ is very surprising, but can be explained quantitatively on the basis of double exchange and strong polaronic effects. Even more surprisingly, the ground state in $(La_{0.5}Nd_{0.5})_{0.67}Ca_{0.33}MnO_3$ can be changed from a metallic to an insulating state upon replacing ^{16}O with ^{18}O. This novel isotope effect clearly demonstrate that charge carriers in the manganites are strongly coupled to the local JT distortions and magnetic moments, so that polarons (quasiparticles dressed by both the local JT distortions and spin polarizations) are formed. Furthermore, we found that both the EPR intensity and linewidth in $La_{1-x}Ca_xMnO_{3+y}$ depend strongly on the oxygen isotope mass, which gives microscopic evidence for the formation of JT polarons in the manganites. Therefore, these isotope effect studies have clarified the nature of charge carriers in manganites, which is crucial to the understanding of the colossal magnetoresistance effect in this system.

10.5.2 Oxygen isotope effect in $La_{2-x}Sr_xCuO_4$

High-temperature superconductivity is known to involve the pairing of charge carriers, but the precise nature of these carriers and the mechanism of their pairing remain unclear. The copper oxides are known to exhibit a strong Jahn-Teller effect and it has been suggested that the charge carriers should be Jahn-Teller polarons [26]. Still, direct evidence that Jahn-Teller polarons exist in the copper oxides has been lacking, although some indirect evidence comes from their recent discovery [32] in the structurally similar but nonsuperconducting manganite $La_{1-x}Ca_xMnO_3$. Recently there has been increasing evidence that polaronic charge carriers are present in the normal-state of the layered cuprates [33, 34]. However, it is not clear whether

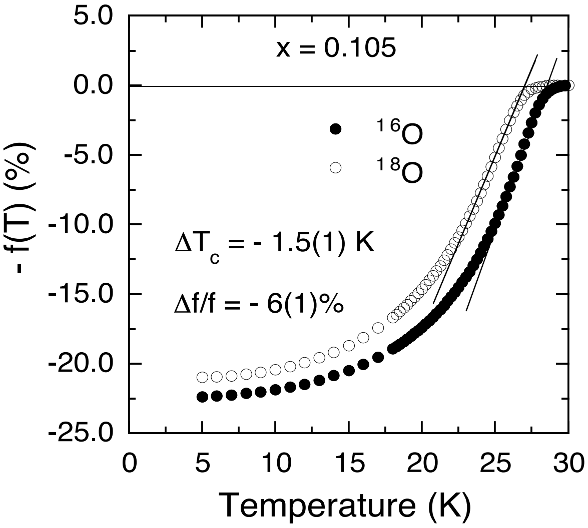

Figure 10.8: Temperature dependence of the Meissner effect for ^{16}O and ^{18}O samples of $La_{2-x}Sr_xCuO_4$ with $x = 0.105$.

these normal-state carriers are Jahn-Teller polarons, and whether they should condense into Cooper pairs.

To show that polaronic charge carriers condense into Cooper pairs, one has to demonstrate that the effective supercarrier mass along the CuO_2 planes (m^*_{ab}) depends strongly on the ionic mass M in these layered cuprate superconductors. In conventional superconductors, only the "bare" carriers condense into the supercarriers, and the supercarrier mass is essentially independent of M. In the polaronic model [28], the effective mass of polarons depends strongly on M. When the polarons condense into supercarriers by whatever pairing mechanism, the effective supercarrier mass will also depend on M. We have performed magnetization and thermal expansion measurements on samples of the one-layer cuprates $La_{2-x}Sr_xCuO_4$, which characterize the oxygen isotope effects on the carrier density and on the in-plane penetration depth. From the oxygen-isotope effect on the Meissner fraction of the decoupled fine-grained samples as shown in Fig. 10.8, we can deduce the oxygen-isotope effect on the in-plane penetration depth. The dependence of the in-plane penetration depth on the oxygen mass is strong in the underdoped samples, and reduced towards the optimal doping. From thermal-expansion measurements, we can study the oxygen isotope effect on the T-O phase transition temperature T_s, which can accurately determine the dependence of the carrier density on the oxygen mass. There is a negligible isotope effect on T_s, and thus on the carrier density. Specific quantitative features of the results show that polaronic charge carriers exist and condense into Cooper pairs in the copper oxide superconductors. The results place strong constraints on the microscopic pairing mechanism of high-T_c superconductivity.

References

[1] G. Blatter *et al.*, Phys. Rev. B **54**, 72 (1996).

[2] S. L. Lee *et al.*, Phys. Rev. Lett. **71**, 3862 (1993).

[3] S. L. Lee *et al.*, Phys. Rev. Lett. **75**, 922 (1995).

[4] S. L. Lee *et al.*, Phys. Rev. B **55** (1997).

[5] C. M. Aegerter *et al.*, Phys. Rev. B **54**, R15661 (1996).

[6] L. I. Glazman and A. E. Koshelev, Phys. Rev. B **43**, 2835 (1991).

[7] B. Khaykovich *et al.*, Phys. Rev. Lett. **76**, 2555 (1996).

[8] V. N. Kopylov *et al.*, Physica C **170**, 291 (1990).

[9] C. M. Aegerter *et al.*, to be published.

[10] S. L. Lee *et al.*, submitted to Phys. Rev. Lett. (1997).

[11] C.C. Tsuei *et al.*, Science **271**, 329 (1996).

[12] J. Annett, N. Goldenfeld, and A.J. Leggett, Physical Properties of High Temperature Superconductors, Vol. 5, D.M. Ginsberg (ed.) (World Scientific, Singapore, 1996).

[13] D.J. Scalapino, Physics Reports **250**, 329 (1995).

[14] A.G. Sun *et al.*, Phys. Rev. Lett. **74**, 797 (1995).

[15] K.A. Müller, Nature **377**, 133 (1995).

[16] Z.F. Ren, J.H. Wang, and D.J. Miller, Appl. Phys. Lett. **73**, 1798 (1996).

[17] M. Tortonese *et al.*, Proceedings of Transucers (1991), and Park Scientific Instruments, Sunnyvale, California.

[18] C. Rossel *et al.*, J. Appl. Phys. **79**, 8166 (1996).

[19] J. Brugger *et al.*, to be published.

[20] A. Shengelaya *et al.*, Phys. Rev. Lett. **77**, 5296 (1996).

[21] K.A. Müller, Phys. Rev. Lett. **2**, 341 (1959).

[22] A. Abragam and B. Bleaney, Electron Paramagnetic Resonance of Transition Ions (Clarendon Press, Oxford, 1970).

[23] J. Karpinski *et al.*, to be published in Physica C (1997).

[24] S. Jin *et al.*, Science **264**, 413 (1994).

[25] R. von Helmolt *et al.*, Phys. Rev. Lett. **71**, 2331 (1993).

[26] K.-H, Höck, H. Nickisch, and H. Thomas, Helv. Phys. Acta. **56**, 237 (1983).

[27] J. G. Bednorz and K. A. Müller, Z. Phys. B**64**, 189 (1986).

[28] A. S. Alexandrov and N. F. Mott, Int. J. Mod. Phys. **8**, 2075 (1994)

[29] A. J. Millis, P. B. Littlewood, and B. I. Shraiman, Phys. Rev. Lett. **74**, 5144 (1995).

[30] P. W. Anderson and H. Hasegawa, Phys. Rev. **100**, 675 (1955).

[31] M. Shikano *et al.*, Solid State Commun. **90**, 115 (1994).

[32] Guo-meng Zhao *et al.*, Nature **381**, 676 (1996).

[33] Proc. Int. Workshop on "Anharmonic Properties of High-T_c Cuprates", edited by D. Mihailowic, G. Ruani, E. Kaldis and K. A. Müller (World Scientific, Singapore, 1994).

[34] X. X. Bi and P. C. Eklund, Phys. Rev. Lett. **70**, 2625 (1993).